Evidences of in vivo bioactivity of Fe-bioceramic composites

by A Kafrawi Nasution

Submission date: 17-Nov-2020 04:18PM (UTC+0800)
Submission ID: 1448798388
File name: vity_of_Fe-bioceramic_composites_for_temporary_bone_implants.pdf (956.99K)
Word count: 8495
Character count: 42711

Society For Biomaterials

Evidences of *in vivo* bioactivity of Fe-bioceramic composites for temporary bone implants

Mokhamad F. Ulum,[1,2] Ahmad K. Nasution,[1,3] Abdul H. Yusop,[1] Andril Arafat,[1] Mohammed Rafiq A. Kadir,[1] Vetnizah Juniantito,[2] Deni Noviana,[2] Hendra Hermawan[1,4]

[1]Faculty of Biosciences and Medical Engineering, University Teknologi Malaysia, Johor Bahru, Malaysia
[2]Faculty of Veterinary Medicine, Bogor Agricultural University, Bogor, Indonesia
[3]Faculty of Engineering, Muhammadiyah University of Riau, Riau, Indonesia
[4]Department of Mining, Metallurgical and Materials Engineering and CHU de Québec Research Center, Laval University, Quebec City, Canada

Received 31 March 2014; revised 28 September 2014; accepted 18 October 2014
Published online 11 November 2014 in Wiley Online Library (wileyonlinelibrary.com). DOI: 10.1002/jbm.b.33315

Abstract: Iron-bioceramic composites have been developed as biodegradable implant materials with tailored degradation behavior and bioactive features. In the current work, *in vivo* bioactivity of the composites was comprehensively studied by using sheep animal model. Five groups of specimens (Fe-HA, Fe-TCP, Fe-BCP composites, and pure-Fe and SS316L as controls) were surgically implanted into medio proximal region of the radial bones. Real-time ultrasound analysis showed a decreased echo pattern at the peri-implant biodegradation site of the composites indicating minimal tissue response during the wound healing process. Peripheral whole blood biomarkers monitoring showed a normal dynamic change of blood cellular responses and no stress effect was observed. Meanwhile, the released Fe ion concentration was increasing along the implantation period. Histological analysis showed that the composites corresponded with a lower inflammatory giant cell count than that of SS316L. Analysis of the retrieved implants showed a thicker degradation layer on the composites compared with pure-Fe. It can be concluded that the iron-bioceramic composites are bioactive and induce a preferable wound healing process. © 2014 Wiley Periodicals, Inc. J Biomed Mater Res Part B: Appl Biomater, 103B: 1354–1365, 2015.

Key Words: biodegradable metals, bioceramics, composites, bioactive, *in vivo*

How to cite this article: Ulum MF, Nasution AK, Yusop AH, Arafat A, Kadir MRA, Juniantito V, Noviana D, Hermawan H. 2015. Evidences of *in vivo* bioactivity of Fe-bioceramic composites for temporary bone implants. J Biomed Mater Res Part B 2015:103B:1354–1365.

INTRODUCTION

Research on biodegradable metals has become one of the most interested fields in biomaterials since its first introduction in early 2000s with iron (Fe) and magnesium (Mg) as the two most studied metals. Improving bioactivity of this new generation of biomaterials is one of the main necessities in developing suitable temporary medical implants. Bioactive materials such as calcium/phosphate (CaP)-based bioceramics were already clinically used owing to their supportive properties toward bone regeneration.[1–3] The excellent bioactivity of hydroxyapatite (HA) and tricalcium phosphate (TCP) bioceramics[4] was reported to be beneficial for cell proliferation, bone ingrowth and osseointegration.[5,6] In their development, these bioceramics were also doped with Fe to form magnetic Fe-HA composites to enhance its regenerative properties for bone surgery and for future anticancer therapies,[7] or to form Fe-modified α-TCP having firm bone bonding for spinal surgery applications.[8] However, bioceramics have higher elastic modulus and lower fracture toughness when compared with human cortical bone.[9,10]

Bioceramics have been added to biodegradable polymers to improve biodegradation such as reduce excessive inflammatory reaction and osteolysis zone.[11–13] Two *in vivo* studies of PLGA-TCP composites have shown preferable biological activities (i.e., bone remodeling and implant degradation) in goat[13] and in rabbit.[12] Incorporating bioceramics into biodegradable metals has recently been viewed as a promising approach to both adding bioactivity of the metals and improving fracture toughness of bioceramics. Coating of bioceramics to biodegradable metals or developing composites of both materials are two envisioned directions. A CaP/chitosan

Correspondence to: H. Hermawan; e-mail: hendra.hermawan@gmn.ulaval.ca or D. Noviana; e-mail: deni@ipb.ac.id
Contract grant sponsor: Indonesian Ministry of Research and Technology for the Insentif Riset SINas; contract grant number: RT-2012-786
Contract grant sponsor: Indonesian Ministry of Education and Culture for the DGHE; contract grant number: 10/IT3.11/LT/2014
Contract grant sponsor: Malaysian Ministry of Education and Universiti Teknologi Malaysia for the Tier-1; contract grant number: Q.J130000.2545.05H55
Contract grant sponsor: Laval University and CHU de Québec for the "Fonds de Démarrage"

composite was coated on porous Fe via electrophoretic deposition as a promising new way to control degradation and bioactivity but further process optimization was needed.[14] Other work has coated pure-Fe with $CaZn_2(PO_4)_2 \cdot 2H_2O$ via chemical reaction method and was found to improve antihemolysis property and cell compatibility.[15] Some biodegradable metal-bioceramic composites have been studied including Mg-HA,[16] Mg-Zn-CaP,[17] Mg-CaP,[18] Fe-Fe_2O_3,[19] and Fe-bioceramics (HA/TCP/BCP).[20] Obviously, they have shown notable enhanced *in vitro* and *in vivo* bioactivity features.[19–21] A composition of 5 wt % (HA/TCP/BCP) in the Fe-bioceramic composites was selected as it resulted into a slight increase of degradation rate compared with pure-Fe while maintaining similar ductility to pure-Fe.[20] However, there is a lack of understanding on their comprehensive bioactive behavior within the body responses. An in-depth assessment on how the entire body responds to these new implants is therefore worth investigating.

Our previous study on the Fe-bioceramic composite implants has shown a good result in their *in vitro* cellular activity and early evidences of a gradual *in vivo* degradation of the implants in the femoral bone of sheep based on radiodensity image analysis.[20,22] The current study aims to further evaluate bioactivity of the Fe-bioceramic composite implants directly in a sheep animal model. Real-time monitoring of their biodegradation was assisted by ultrasound imaging on the peri-implant tissue region combined with peripheral blood biomarkers and histological analysis for biodegradation and tissue compatibility analysis. The retrieved implants were also analyzed to obtain supporting evidence of bioactivity and biodegradation process.

MATERIALS AND METHODS

Preparation of the iron-bioceramic composites implant

The Fe-bioceramic composites were prepared through powder metallurgy from powders of pure-Fe, hydroxyapatite (HA) and tricalcium phosphate (TCP) as reported elsewhere.[20] In brief, samples were prepared by firstly mixing the starting powders with the following composition of (1) 100 wt % Fe (pure-Fe); (2) Fe-5 wt % HA (Fe-HA); (3) Fe-5 wt % TCP (Fe-TCP); and (4) Fe-5 % wt (60% HA:40% TCP) (Fe-BCP). Each mixture was uniaxially pressed into pellets (12.67 mm in diameter) under 13.8 MPa compression pressure. The pellets were then sintered under vacuum at 1100°C for 1 h and cooled to room temperature. The sintered pellets were then cut to produce implant specimens ($5 \times 2 \times 0.5$ mm^3). Stainless steel 316L was used as a control. The specimen surface was successively ground using SiC abrasive paper up to grit #2000 and ultrasonically washed in 75% alcohol and distilled water. Further sterilization was performed before implantation using oven sterilization at 160°C for 60 min that was found to be effective in damaging microorganism on the implants or surgical tools.[23]

Animal surgical implantation and wound healing monitoring

Five male Indonesian thin tailed sheep (age 10–12 month, weight 14–16 kg) were used in this study with ethical clearance from Bogor Agricultural University Animal Care and Use Ethics Committee (ACUC No: 03–2012 IPB). The sheep model was chosen because of its similarity to humans in terms of bone turnover and remodelling activity.[24] The sheep received premedication (Atropine®, 0.06 mg/kg iv, Indofarma, Indonesia) after 24 h of fasting and induced with general anaesthesia (Ilium Xylazine-20®, 0.1 mg/kg iv, Troy Laboratories, Australia) 10 min later and continuously maintained in this condition. The surgery was started with drilling and flattening bone defects below the radius periosteum membrane of radial forelegs on medio proximal region. The implants were inserted into the defects where one sheep received one implant on each leg. The surgical wound was closed with suture (Vicryl®, Ethicon, USA) and bandage (Hypafix®, BSN Medical, Sweden). General antibiotic (Novamox-G®, 1 mL/10 kg, Nova Laboratories, Malaysia) and topical spray antibiotic (Limoxin-25 spray®, Interchemie Werken, Holland) were given for the first 6 days to avoid postoperative infection. The surgical wound healing at the implantation sites was monitored and photographed at day 9, 14, and 35 postimplantation. Thickness of the tissue swelling at the implantation sites was quantified by using a computer-aided image analysis software (ImageJ, National Institutes of Health, USA) from the photographs ($n = 5$). None of the sheep was sacrificed until the end of the study.

Peri-implant biodegradation monitoring

The peri-implant implant biodegradation was monitored non-invasively by using real-time 2D ultrasound method. Longitudinal view of Brightness-mode (B-mode) ultrasound was performed on each sheep by using a SonoDop ultrasound console (Karindo Alkesteron, Indonesia) with linear multi-frequency transducer (7.5–15 MHz). The B-mode scan probe was gently placed on the skin surface perpendicular to the implantation site by using ultrasonic transmission gel. Reflected ultrasonic waves (echo) were captured and optimal transectional implant images of the on-screen real-time movie were captured. The ultrasound evaluation was performed at day 3, 9, 35, and 60 postimplantation. The images were further analyzed by using plot profile module in ImageJ software at the mid of echo-pattern side-to-side (along the implant length) ($n = 5$).

Blood biomarker monitoring

Systemic response to the implantation was monitored by evaluating biomarkers in the peripheral blood samples at day 3, 9, 14, 35, 50, and 60 postimplantation. Five mililiter of venous blood was collected at jugular vein of each sheep into vacutainer with ethylene diamine tetraacetic acid (EDTA) anticoagulant. For routine hematology, 0.5 mL whole blood samples were examined for the numbers of red blood cells (RBC), hemoglobin (Hb), hematocrit (PCV), white blood cells (WBC), and WBC differentiation cells. Stress response postimplantation was analysed by measuring the ratio of Neutrophil (N) to Leukocyte (L) cell count. The remaining whole blood samples were centrifuged at 1000 rpm for 10 min to separate the blood plasma. Concentration of Fe and Ca in the blood plasma was measured by using an AA-7000

atomic absorption spectrophotometer (Shimadzu, Japan) and concentration of P was quantified by using molybdovanadate method and a 200RS UV spectrometer (LW Scientific, USA) at 660 nm.

Histological evaluation

A standardized balanced anaesthetic and surgical approach protocol was used as explained in the previous section. After incising the implantation site, the bone around the implant was drilled down till bone marrow to recover biopsy tissue samples for histological examination. The remnant implants were explanted from biopsy tissue, dried and stored in desiccated tubes for further visual and chemical analysis. The biopsy tissue samples were fixed in buffered neutral 10% formaldehyde, decalcified in 5% nitric acid for 7 days, dehydrated stepwise through ascending series of alcohol solutions and finally degreased in xylene. The tissues were then embedded in paraffin block, sliced at 5 μm by microtome, and stained using hematoxylin and eosin (HE) stains. Cell response at the peri-implant tissues was observed under a CH30 optical microscope (Olympus, Japan) and histological images were captured and analyzed.

Retrieved implant evaluation

The explanted remnant implants were analyzed for surface morphology, chemical composition and thickness of degradation layer by using a TM3000 SEM/EDS (Hitachi, Japan). Surface roughness of the remnant implants was also determined by LEXT OLS4000 laser scanning confocal microscope (Olympus, USA). Arithmetical mean deviation of the profile (Ra) was obtained in terms of the surface roughness measurement with an evaluation length of 4 mm and five samples.

Statistical analysis

Statistical analysis was performed by using a one-way ANOVA with a post hoc Duncan test using SPSS v.16.0 software (SPSS Inc., USA) at the 95% confidence level. A p-value of <0.05 was considered as statistically significant.

RESULTS

Implantation and visual wound healing observation

Figure 1 shows the implant insertion, example of wound healing process for Fe-HA implants and peri-implant extraction. After implantation, all animals remained active and were not disturbed with the presence of the implant in their sub-periosteum leg bones [Figure 1(a)]. Black colored degradation product was observed within the incised biopsy [Figure 1(b)]. Wound healing observation showed swelling (inflammation) process which was no longer observed 35 days postimplantation [Figure 1(c–e)].

Table I shows tissue swelling thickness at the implantation sites measured from the images as shown in Figure

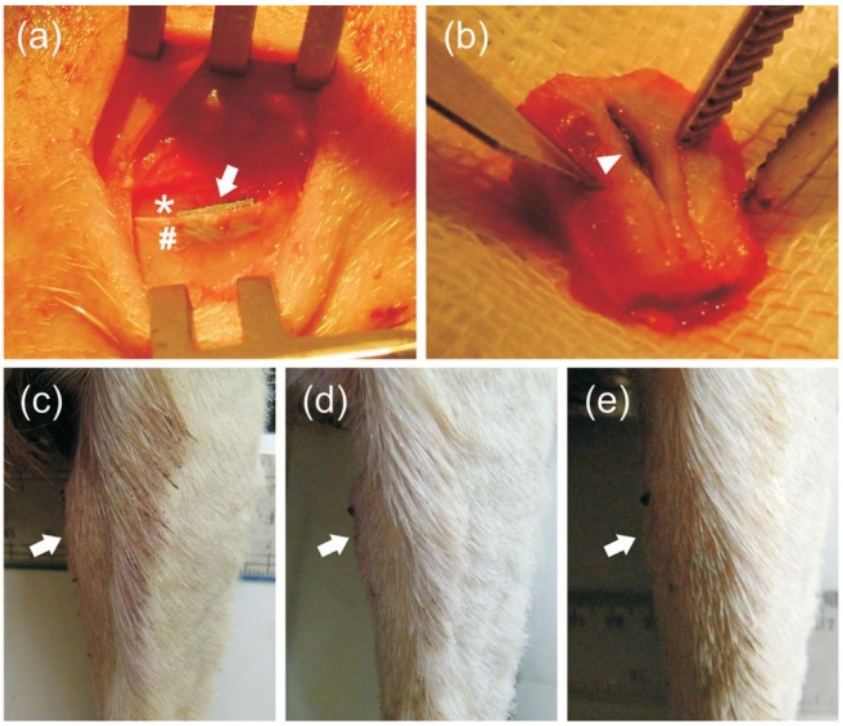

FIGURE 1. Implant insertion, extraction and wound healing observation showing: (a) implantation in sub-periosteum leg bones showing implant (arrow), bone (*), periosteum (#), (b) extraction of biopsy showing biodegradation product (arrow head), (c, d, e) wound healing observation of Fe-HA implants at day 9, 14, and 35, respectively, showing implantation sites (arrow). [Color figure can be viewed in the online issue, which is available at wileyonlinelibrary.com.]

TABLE I. Tissue Swelling Thickness (mm) at Implantation Sites

	Implant Group				
Day	Pure-Fe	Fe-HA	Fe-TCP	Fe-BCP	SS316L
Day 0	0.0 ± 0.0^{a}	0.0 ± 0.0^{a}	0.0 ± 0.0^{a}	0.0 ± 0.0^{a}	0.0 ± 0.0^{a}
Day 9	2.1 ± 0.1^{d}	2.2 ± 0.1^{d}	3.4 ± 0.1^{g}	1.7 ± 0.1^{c}	5.2 ± 0.1^{h}
Day 14	1.8 ± 0.1^{c}	3.4 ± 0.1^{g}	2.7 ± 0.1^{e}	1.7 ± 0.0^{c}	3.1 ± 0.1^{f}
Day 35	0.0 ± 0.0^{a}	0.0 ± 0.0^{a}	0.9 ± 0.1^{b}	1.0 ± 0.0^{b}	0.0 ± 0.0^{a}

Data shown as mean with standard deviation ($x \pm SD$). The same letter in a different row and column shows the differences were not significant ($p > 0.05$).

1(c–e) as a quantitative visual measure of tissue response. It can be seen that the degree of tissue response follows the trend of Fe-BCP < Fe-HA = pure-Fe < Fe-TCP < SS316L.

B-mode ultrasound observation

Figure 2 shows the B-mode sonograms of each implant at different implantation period. Hypoechoic pattern is observed at the top side of pure-Fe implant (muscle-implant side) indicating an inflammation response in the area. Anechoic pattern is produced when the ultrasound passed through fluid of soft tissue (i.e., inflammation fluid) and because there is no (anechoic) or minimal (hypoechoic) reflection it forms a black to gray color in the sonograms. The anechoic pattern was

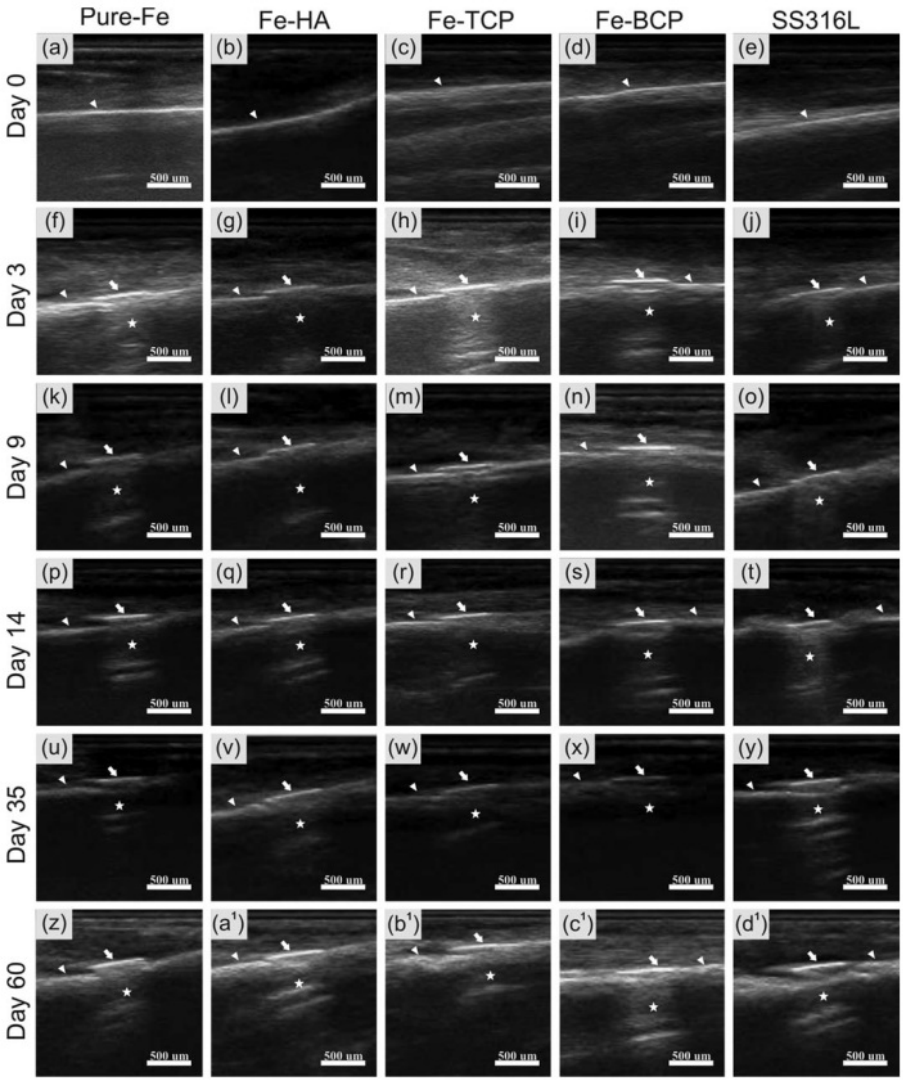

FIGURE 2. Sonogram of the implants at different days postimplantation. Note: "arrow" = implant, "arrow head" = bone, "star" = comet-tail artefact at the bottom of implant in the bone marrow.

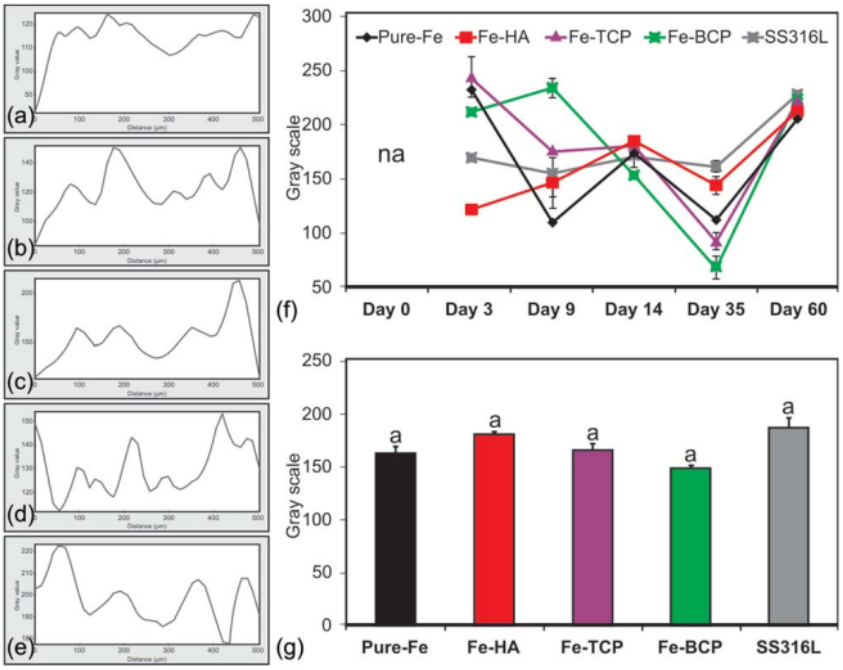

FIGURE 3. Sonogram analysis: (a-e) plots of echogenicity peaks against length of Fe-HA implants at day 3, 9, 14, 35, and 60, respectively, (f) average peak height (gray scale) of the implants at different days postimplantation, (g) mean value of peak height of day 14, 35, and 60. Note: "na" = not applicable, the same letter in a different bar shows the differences were not significant ($p > 0.05$). [Color figure can be viewed in the online issue, which is available at wileyonlinelibrary.com.]

more pronounce until day 60 for the SS316L compared with that of pure-Fe and Fe-bioceramics. The Fe-bioceramic composite implants also showed hyperechoic pattern (white colored because of highly reflected sound by hard materials such as bone, metals or gas) from day 3 to 14 but decreased at day 60. Meanwhile, the SS316L implant showed increasing hyperechoic pattern at all times of observation. The pattern for the bottom side of implants (bone-implant side) cannot be evaluated because of insufficient echo to make a good image which correlates with the highly reflected surface of metallic material. This condition leads to the formation of comet-tail artefact hyperechoic patterns which produced white color in the sonograms. Thus, these comet-tail artefact hyperechoic patterns cannot be used to distinguish implant degradation and tissue interactions at the bottom side of the implants.

Figure 3 shows an example of further sonogram analysis for Fe-HA implant by using ImageJ software plotting the peaks of echogenicity against the length of implants [Figure 3(a–e)]. The average peak height (gray scale) was then compared for each implant at different days postimplantation [Figure 3(f, g)]. This analysis suggests a semi-quantitative measure of biodegradation progress at the implant surface.

During the first 14 days postimplantation, the echo patterns of pure-Fe and Fe-bioceramics show a distinct peak variation in contrast to SS316L [Figure 3(f)]. This fact suggests a more active tissue response toward Fe-bioceramics (bioactive) compared with SS316L (inert). In addition, degradation product formed on the former and should not be the case for the latter. At day 35, peak variation decreased with the Fe-BCP showing the lowest. The peak variation increased again at day 60 with almost similar for all group. Figure 3(g) shows the mean value of peak height of combined day 14, 35, and 60 indicating Fe-BCP implant has more active biodegradation behavior compared with other bioactive implants.

Blood cell count

Table II details the number of red blood cell (RBC), hemoglobin (Hb), hematocrit (PCV), white blood cells (WBC), and white blood differentiation cells. It can be seen that the RBC, Hb and PCV counts are in the normal range for any time of implantation. In detail, the average RBC count of Fe-TCP and SS316L at day 60 is higher than those of Fe-BCP, pure-Fe and Fe-HA groups. The Hb and PCV for Fe-TCP is the lowest among all groups.

The number of WBC at averaged day 14 decreases following the trend: Fe-BCP>Fe-HA>pure-Fe>SS316L>Fe-TCP. Interestingly, the Fe-BCP implant showed the biggest decrease of WBC number from averaged day 14 to averaged day 60. Further analysis on white blood differentiation cells of the Fe-BCP revealed that agranulocyte cells (i.e., lymphocyte and monocyte) have higher number at averaged day 14 but again decreased at averaged day 60. The N/L ratio of pure-Fe and Fe-bioceramic groups is below 1.5, which is a

TABLE II. Blood Cell Count

Cells	Implants Group									
	Pure-Fe		Fe-HA		Fe-TCP		Fe-BCP		SS316L	
	Avday 14	Avday 60	Avday 14	Avday 60	Avday 14	Avday 60	Avday 14	Avday 60	Avday 14	Avday 60
RBC (10^6 cells/μL)	13.0 ± 1.9^{bcd}	12.6 ± 1.4^{abcd}	11.0 ± 1.8^{ab}	11.9 ± 0.9^{abc}	10.0 ± 2.0^{a}	14.4 ± 2.6^{cd}	12.4 ± 2.3^{abcd}	13.0 ± 1.0^{bcd}	9.9 ± 1.9^{a}	14.9 ± 1.4^{d}
Hb (g/dL)	9.9 ± 0.8^{ab}	10.8 ± 0.8^{ab}	9.7 ± 0.4^{ab}	10.4 ± 1.3^{ab}	8.7 ± 0.1^{a}	9.3 ± 1.3^{ab}	9.8 ± 0.8^{ab}	11.4 ± 3.3^{b}	9.8 ± 0.5^{ab}	11.4 ± 0.8^{b}
PCV (%)	27.8 ± 2.5^{bcd}	28.5 ± 2.5^{bcde}	27.0 ± 1.7^{bc}	28.7 ± 1.3^{bcde}	23.3 ± 0.9^{a}	26.4 ± 1.0^{b}	26.5 ± 1.8^{bc}	31.0 ± 2.2^{e}	27.2 ± 1.3^{bc}	30.4 ± 0.5^{de}
WBC (10^3 cells/μL)	15.0 ± 5.3^{bc}	11.0 ± 1.4^{ab}	16.0 ± 2.5^{c}	10.6 ± 2.1^{ab}	8.9 ± 0.8^{a}	8.9 ± 1.9^{a}	21.0 ± 5.7^{d}	12.4 ± 4.3^{abc}	13.5 ± 2.7^{abc}	11.0 ± 2.8^{ab}
Agranulocyte (%WBC)	52.3 ± 14.2^{ab}	56.8 ± 17.2^{ab}	50.0 ± 27.8^{ab}	46.5 ± 18.4^{ab}	64.7 ± 14.4^{b}	60.3 ± 28.0^{ab}	55.7 ± 8.1^{ab}	44.5 ± 20.4^{ab}	46.7 ± 5.9^{ab}	33.5 ± 15.0^{a}
Granulocyte (%WBC)	47.7 ± 14.2^{ab}	43.3 ± 17.2^{ab}	50.0 ± 27.8^{ab}	53.5 ± 18.4^{ab}	35.3 ± 14.4^{a}	39.8 ± 28.0^{ab}	44.3 ± 8.1^{ab}	55.5 ± 20.4^{ab}	53.3 ± 5.9^{ab}	66.5 ± 15.0^{b}
Lymphocyte (%WBC)	49.3 ± 13.2^{ab}	55.5 ± 17.7^{ab}	48.3 ± 29.4^{ab}	44.5 ± 18.7^{ab}	63.0 ± 15.0^{b}	57.0 ± 27.4^{ab}	53.3 ± 7.6^{ab}	42.5 ± 18.4^{ab}	44.7 ± 6.7^{ab}	32.0 ± 14.8^{a}
Monocyte (%WBC)	3.0 ± 1.0^{a}	1.3 ± 0.5^{a}	1.7 ± 1.5^{a}	2.0 ± 1.2^{a}	1.7 ± 0.6^{a}	3.3 ± 3.9^{a}	2.3 ± 0.6^{a}	2.0 ± 2.2^{a}	2.0 ± 1.0^{a}	1.5 ± 1.0^{a}
Basophil (%WBC)	NIL^{a}	NIL^{a}	NIL^{a}	NIL^{a}	NIL^{a}	NIL^{a}	NIL^{a}	NIL^{a}	NIL^{a}	NIL^{a}
Neutrophil (%WBC)	41.0 ± 10.0^{ab}	39.3 ± 17.4^{ab}	46.7 ± 25.2^{ab}	46.3 ± 16.7^{ab}	27.7 ± 9.5^{a}	33.0 ± 27.9^{a}	36.3 ± 6.4^{ab}	46.0 ± 21.4^{ab}	51.3 ± 5.1^{ab}	63.0 ± 14.3^{b}
Eosinophil (%WBC)	6.7 ± 4.6^{ab}	4.0 ± 0.82^{ab}	3.3 ± 2.9^{ab}	7.5 ± 3.8^{ab}	7.7 ± 6.1^{ab}	6.8 ± 1.5^{ab}	8.0 ± 2.0^{ab}	9.5 ± 7.7^{b}	2.0 ± 1.0^{a}	3.5 ± 3.1^{ab}
Neutrophil/Lymphocyte	0.9 ± 0.5^{ab}	0.9 ± 0.8^{ab}	1.5 ± 1.5^{ab}	1.3 ± 0.8^{ab}	0.5 ± 0.2^{a}	1.1 ± 1.5^{ab}	0.7 ± 0.2^{a}	1.4 ± 0.9^{ab}	1.2 ± 0.3^{ab}	2.6 ± 2.0^{b}

Data shown as mean with standard deviation (x ± SD). The same letter in a different row shows the difference was not significant ($p > 0.05$). Avday 14 = value compiled and averaged from data of day 3, 9, and 14; Avday 60 = value compiled and averaged from data of day 35, 50, and 60.

normal ratio for both averaged days 14 and 60. Meanwhile, the N/L ratio for SS316L at the averaged day 60 is 2.6, which is higher than normal.

Ion concentration in the blood plasma

Table III details ion concentration in the blood plasma released during the implant degradation. The pure-Fe implant released the highest Fe ion concentration followed by Fe-BCP and others. In all groups, Fe and P concentrations decreased from averaged days 14 to 60, whereas the Ca increased. Meanwhile, the Ca/P ratio shows a consistent slight increase from averaged days 14 to 60 for all groups without a significant difference. Ca/P ratio is one of the inflammation biomarker assessments indicating the

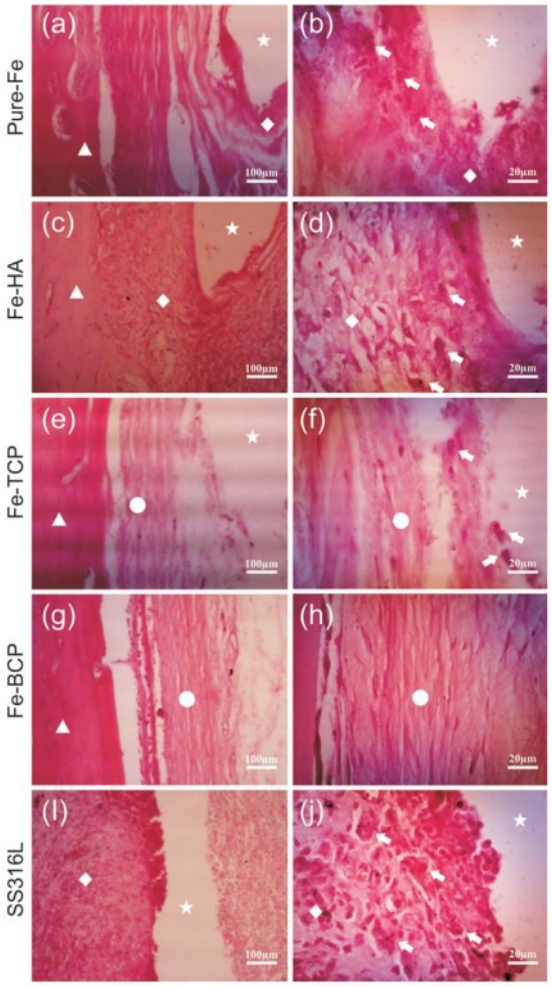

FIGURE 4. Histological images around the implants at day 70: (a, b) pure-Fe, (c, d) Fe-HA, (e, f) Fe-TCP, (g, h) Fe-BCP, (i, j); SS316L. Note: "triangle" = bone, "circle" = fibrous tissue, "diamond" = granular tissue, "star" = void after implant removal, "arrow" = giant cells. [Color figure can be viewed in the online issue, which is available at wileyonlinelibrary.com.]

inflammation responses by the host, which is normally around 2.5.

Histological observation

Figure 4 shows histological images of Fe-bioceramics implants at day 70 postimplantation. The inflammatory giant cells (macrophages) are observed on the tissue around pure-Fe, Fe-HA, Fe-TCP and SS316L implants, but less pronounced around the Fe-BCP. Granular tissue appeared clearly around the SS316L but less pronounced around the pure-Fe and Fe-bioceramic. Interestingly, no granular tissue is observed around the Fe-TCP and Fe-BCP implants. Fibrous tissue appearance consistently increased over time of implantation with the greatest formation found around the Fe-BCP implant.

Retrieved implants observation

Figure 5 depicts surface morphology of the retrieved implants showing the degradation product formation on the implant surfaces. Table IV details the thickness of degradation layer measured from the SEM images of implant's cross section. The thickness increased with prolonged implantation time. The EDS analysis (Figure 5 inset) indicated an increasing content of Fe and O and a decreasing content of Ca and P on the degradation layer of Fe-bioceramic implants as the implantation time prolonged, indicating the progress of degradation. Meanwhile, surface roughness measurement on the retrieved implants at day 70 (Figure 6) revealed that the Fe-BCP has the highest roughness among other implants.

DISCUSSION

Local tissue response to the implantation of Fe-bioceramic composites

Right after the surgical implantation, the implants were continuously exposed to the tissue/body fluid and cells that are activated by the acute wound healing process.[25] Bioactive implants, that is bioceramics and biodegradable polymers, induce more cellular activity at the material-tissue interface.[26] It begins with the entering of WBC to the tissue from the circulatory blood cells. The first WBC (i.e., neutrophil cells) enters the wound site and begins to phagocyte the damaged tissue, bacteria and foreign materials within days. Then inflammatory reaction occurs by recruiting monocytes (macrophages) to prolong the phagocytosis until the material has been completely degraded which may require months to several years.[27] Consecutively, proliferative process begins with the migration of fibroblasts to the wound site to deposit new extracellular matrix. Finally, the wound healing process ends by the encapsulation of the residual materials by new collagen matrix.

Previous studies on metal-bioceramic composites (i.e., Mg-HA and Fe-HA) have showed signs of enhanced cellular activity (i.e., phagocytosis) toward active degradation process of the composite implants.[16,20] However, the understanding of *in vivo* biodegradation process of these composites is still limited. Our results showed that the

TABLE III. Ion Concentration in the Blood Plasma

	Implant Group									
	Pure-Fe		Fe-HA		Fe-TCP		Fe-BCP		SS316L	
Ions (ppm)	Avday 14	Avday 60	Avday 14	Avday 60	Avday 14	Avday 60	Avday 14	Avday 60	Avday 14	Avday 60
Fe	12.8 ± 8.7^{b}	4.6 ± 4.3^{a}	9.3 ± 4.6^{ab}	4.4 ± 2.9^{a}	9.2 ± 1.5^{ab}	3.7 ± 0.6^{a}	10.4 ± 6.2^{ab}	4.6 ± 3.3^{a}	6.7 ± 1.0^{ab}	5.2 ± 2.8^{a}
Ca	518.9 ± 146.2^{abc}	664.9 ± 15.4^{d}	500.2 ± 146.2^{abc}	658.9 ± 45.4^{d}	452.3 ± 122.5^{a}	$618.7 \pm 27.9b^{cd}$	506.1 ± 144.6^{abc}	638.0 ± 13.8^{cd}	494.0 ± 123.3^{ab}	635.4 ± 24.4^{bcd}
P	197.2 ± 33.9^{b}	159.1 ± 44.6^{ab}	164.9 ± 34.4^{ab}	150.5 ± 9.4^{ab}	209.4 ± 87.9^{b}	198.3 ± 49.8^{b}	215.4 ± 73.1^{b}	174.9 ± 38.1^{b}	193.0 ± 66.4^{b}	191.1 ± 37.9^{b}
Ca/P	2.6 ± 4.3^{a}	4.2 ± 0.4^{a}	3.0 ± 4.3^{a}	4.4 ± 4.9^{a}	2.2 ± 1.4^{a}	3.1 ± 0.6^{a}	2.4 ± 2.0^{a}	3.7 ± 0.4^{a}	2.6 ± 1.9^{a}	3.3 ± 0.7^{a}

Data shown as mean with standard deviation ($x \pm SD$). The same letter in a different row shows the difference was not significant ($p > 0.05$). Avday 14 = value compiled and averaged from data of day 3, 9, and 14; Avday 60 = value compiled and averaged from data of day 35, 50, and 60.

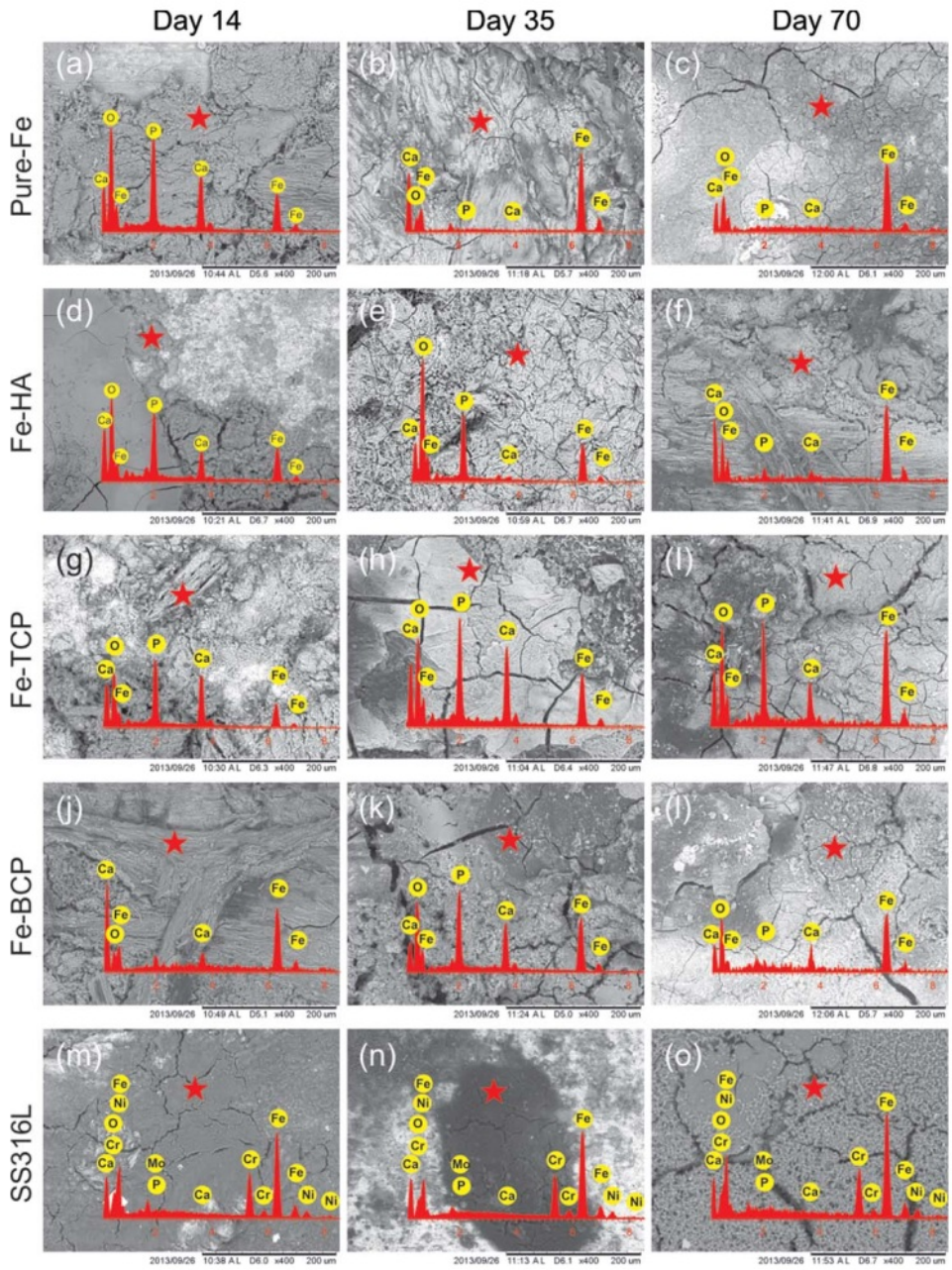

FIGURE 5. SEM images and EDS spectra (inset) showing surface morphology of the retrieved implants at different days postimplantation. Note: "star" indicates the location of EDS analysis. [Color figure can be viewed in the online issue, which is available at wileyonlinelibrary.com.]

Fe-bioceramic composite implants exhibited higher bioactivity compared with pure-Fe and SS316L. The wound healing observation showed that the composites produced an extended swelling (Table I) indicating a prolonged cellular activity around the composite implants. This will be explained in more detail in relation to the blood biomarkers count in the next section. From the ultrasound assessment (Figure 2), the tissue swelling correlated with the decreasing echogenicity in the sonograms of the composite implants with the bioactive TCP (Fe-TCP and Fe-BCP) producing the greatest decrease. The anechoic pattern (black colored images) on the upper peri-implant site indicated an

TABLE IV. Thickness of the Degradation Layer

Thickness (μm)	Implant Group				
	Pure-Fe	Fe-HA	Fe-TCP	Fe-BCP	SS316L
Day 0	0.0 ± 0.0^{a}	0.0 ± 0.0^{a}	0.0 ± 0.0^{a}	0.0 ± 0.0^{a}	0.0 ± 0.0^{a}
Day 14	23.5 ± 0.7^{d}	44.5 ± 2.8^{h}	44.6 ± 2.5^{h}	25.8 ± 0.8^{e}	11.2 ± 1.5^{b}
Day 35	41.4 ± 0.8^{g}	30.1 ± 0.8^{f}	23.9 ± 0.9^{de}	43.0 ± 1.2^{gh}	12.0 ± 0.6^{b}
Day 70	28.5 ± 1.6^{f}	41.1 ± 1.4^{g}	30.1 ± 1.5^{f}	73.5 ± 3.9^{i}	20.4 ± 0.8^{c}

Data shown as mean with standard deviation ($x \pm SD$). The same letter in a different row and column shows the differences were not significant ($p > 0.05$).

accumulation of extra cellular body fluid resulted from more pronounced inflammation reaction around the composite implants.[28] The lower peri-implant side showed a hyperechoic pattern (bright image) with a comet-tail artefact.[29] Along with the prolonged implantation time, especially for the composite implants, the artefact became less visible. Further quantitative analysis (Figure 3) plots the echogenicity peaks against the length of the implants which shows that Fe-BCP degraded more. This finding is in agreement with the similar finding of higher activity of BCP compared with TCP.[30] Moreover, the Fe-BCP implants produced lower peaks compared with other implants which can be related to the tissue reaction toward surface condition (i.e., degradation layer) as shown on the retrieved implants (Figure 5).

The histological analysis (Figure 4) shows similar cellular activity around the composite implants but with less granular tissue formation around Fe-TCP and Fe-BCP (the least) implants compared with that of Fe-HA and SS316L. Normally, the occurrence of inflammatory reaction and fibrous tissue formation during the first 14 days are the normal responses toward implantation to heal the damaged tissue.[31,32] The number of macrophages cells recruited from the circulatory blood monocyte cells were found higher for the Fe-HA implant than others (Table II). This can be related to the fact that HA has the ability to induce more inflammation than TCP.[33]

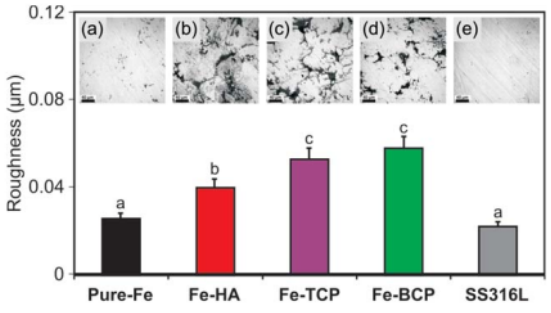

FIGURE 6. Average surface roughness of the retrieved implants and (insets a-e) surface appearance of pure-Fe, Fe-HA, Fe-TCP, Fe-BCP and SS316L implants, respectively. Note: the same letter in a different bar shows the differences were not significant ($p > 0.05$).[Color figure can be viewed in the online issue, which is available at wileyonlinelibrary.com.]

Circulatory system response

Once an implant is placed *in vivo*, blood is the first to come into direct contact. A monolayer of protein is then formed on the implant surface within a few seconds which then interacts with platelets and mesenchymal cells.[25] This contact results into a series of biological processes such as protein deposition, coagulation, inflammation, and tissue formation.[34] Therefore, evaluating blood biomarkers is a way to understand body response to implantation of biomaterials, that is, toxicity (RBC number), rejection (WBC number) and cellular stress response (N/L ratio).[35]

Table II shows that the RBC numbers are within the normal range indicating no toxicity tendency occurred in the sheep for all groups of implants. Meanwhile, WBC test shows different counts for all implant groups. The Fe-HA implant correlates with higher number of WBC than those of Fe-TCP and Fe-BCP. Again, this can be related to the fact that bioactive HA has more pronounced pro-inflammatory properties than TCP.[33] The granulocytes cells (i.e., neutrophils and eosinophil) are found to be dominant in the circulatory WBC for the Fe-HA implant, whereas agranulocytes cells (i.e., lymphocytes and monocytes) are more dominant for the Fe-TCP and Fe-BCP. Fewer circulatory monocytes were found for Fe-HA implant compared with those of Fe-TCP and Fe-BCP. Monocyte cells are the precursor for macrophage and will be recruited into the surrounding implant during inflammation reaction.[36,37] High number of monocyte in the circulatory blood indicates less monocyte is recruited to infiltrate the tissue. This is related to the histological analysis which found more macrophage cells at the peri-implant tissue (granular tissue) of Fe-HA. Moreover, this blood biomarker count also supports that Fe-bioceramic implants induced more cellular activities compared with the pure-Fe and SS316L and also supports the observation of the extended swelling for Fe-bioceramic implants during the wound healing process.

Another analysis is by comparing the neutrophil cell count to lymphocyte (N/L ratio) which indicates cellular stress responses.[38] In our study, the N/L ratio (Table II) is in the range of normal value as suggested by other work[39] indicating no cellular (body) stress occurred after implantation of the Fe-bioceramic and pure-Fe implants. In more detail the N/L ratio of Fe-HA is higher than those of Fe-TCP and Fe-BCP implants.

Biodegradation process of the implants releases ions into the adjacent tissue passively then subsequently changes

ion concentration in the blood plasma.[35,40] Table III shows that pure-Fe implant released more Fe ion than the other implants in the first 2 weeks postimplantation. However, the Fe ion concentration in the sheep blood plasma for all groups is still in the normal value.[41] The content of 5 wt % bioceramic in the Fe-bioceramic composites is found to have no influence on the Ca and P concentration in blood plasma. The Ca/P ratio is around the normal level indicating a mild degree of inflammation for all Fe-bioceramic implants. Inflammation will normally cause a decrease of Ca/P ratio because of imbalance of body Ca and P mineral.[42,43] The released Ca and P from the Fe-bioceramic implants may help to bring back the Ca/P ratio to the normal level by the body homeostasis system.[44]

Implant retrieval analysis

Metal that is implanted *in vivo* undergoes both passive and active degradation because of the electrochemical reaction of the material with body fluid[45] and to cellular activity by the macrophage that involves phagocyting the biodegradation product at the implant surface. Our previous study showed that the addition of bioceramics to pure-Fe has shifted its potential toward more active region,[20] which was also observed on Mg alloy.[46] The degradation layer of Fe-bioceramics is thicker than that of pure-Fe (Table IV) indicating more degradation and cellular activity occurred on the former. This is correlated with the ultrasound image of the Fe-bioceramic implants, especially Fe-TCP and Fe-BCP, which produced a decreasing echogenicity on the comet-tail artefact pattern (Figures 2 and 3). The thicker degradation layer of Fe-BCP implant is related to the higher degradation rate of BCP and TCP compared with HA in body environment.[47,48] The thicker degradation layer may contribute to tissue swelling during wound healing where swelling thickness was thicker for Fe-bioceramics than pure-Fe implant (Table I). However, the swelling was found to be thinner on the Fe-bioceramics after 35 days postimplantation.

The more active behavior of Fe-bioceramic implants was also marked by the increasing content of Fe and O on the degradation layer (Figure 5), especially on the Fe-BCP. The bioceramic-Fe interface on the Fe grain boundaries may have facilitated fluid imbibition into the bulk because bioceramics are hydrophilic.[49] Therefore the Fe-bioceramic implants degraded from both external and internal attack. The increasing degradation layer thickness of the Fe-bioceramics (Table IV) correlates with the decreasing echogenicity pattern plotted along the implant length (Figure 3). The Fe-bioceramic implants were also characterized by a rougher surface than pure-Fe and SS316L implants (Figure 6). This could be related to higher cellular activity on the Fe-bioceramic implants that formed biofilms mainly consisting of Ca/P precipitate.[50,51] A rougher surface was found to be beneficial in enhancing bone-to-implant contact[52] and in determining the balance between bone formation and resorption at the interface of the bone implant.[6,53]

Interestingly, from this study, we can see the synergistic influence of HA and TCP combination on the bioactivity as shown by the Fe-BCP composite. HA has been reported to have a low bioresorbability[43] and is suspected to have a role in blocking new bone formation and remodeling[54] in contrast to TCP.[30] A combination of 80% HA and 20% TCP has been found to have no difference toward bone regeneration.[55] However, based on our results, the 60% HA and 40% TCP combination resulted in a more active behavior of the Fe-BCP implant compared with Fe-HA and Fe-TCP.

Apart of degradation and bioactivity, another important concern that has not been addressed in this work is MRI compatibility of the Fe-bioceramic composites. In fact, this concern has never been rigorously addressed in the study of Fe-based biodegradable metals except for few studies. Magnetic susceptibility of biodegradable Fe-(20–35 wt %) Mn alloys were tested as an indirect measure to MRI compatibility and the alloys were reported to have lower magnetic susceptibility than that of SS316L as a result of the Mn alloying that produced antiferromagnetic austenitic phase.[56] However, some preclinical studies of iron stents seem not much concerned with MRI compatibility issue probably because of the consideration that these biodegradable implants present only temporary in the body.[57–59] Indeed, Fe has been doped into HA to form Fe-HA composites endowed with superparamagnetic ability for utilization as active scaffold for bone regeneration or as nontoxic biodegradable magnetic nanocarriers for hyperthermia-based anticancer treatments.[7,60–62]

CONCLUSION

In vivo bioactivity of iron-bioceramic composites (Fe-HA, Fe-TCP, and Fe-BCP) was studied and compared with pure-Fe and SS316L. The local tissue response (ultrasound and histology), circulatory biomarkers and implant retrieval analysis results showed that the composite implants had an enhanced bioactivity and biodegradation behavior compared with the pure-Fe implant. The composite implants maintained a normal dynamic blood biomarker change and did not induce stress effect. The ultrasound analysis showed evidence of more active biodegradation of Fe-BCP compared with other implants. Granular tissue formation was less pronounced around the Fe-BCP than around the other implants with the number of macrophage cell higher for the Fe-HA implant. The content of 5 wt % bioceramic in the composites showed no influence on the Ca and P concentration in the blood plasma indicating a mild degree of inflammation for all composite implants. The thicker degradation layer and rougher surface of the retrieved composite implants supported the finding of enhanced bioactivity of the composites with the Fe-BCP found to be the most active. The combination of 60% HA and 40% TCP is viewed as the reason for the higher bioactivity of the Fe-BCP compared with other Fe-bioceramic composite implants.

REFERENCES

1. Kamitakahara M, Ohtsuki C, Miyazaki T. Review paper: Behavior of ceramic biomaterials derived from tricalcium phosphate in physiological condition. J Biomater Appl 2008;23:197–212.

2. Surmenev RA, Surmeneva MA, Ivanova AA. Significance of calcium phosphate coatings for the enhancement of new bone osteogenesis: A review. Acta Biomater 2014;10:557–579.
3. Shen JZ, Fäldt J. Chapter 13: Requirements of bioactive ceramics for dental implants and scaffolds. In: Shen JZ, Kosmač T, editors. Advanced Ceramics for Dentistry. Oxford: Butterworth-Heinemann; 2014. pp 279–300.
4. Samavedi S, Whittington AR, Goldstein AS. Calcium phosphate ceramics in bone tissue engineering: A review of properties and their influence on cell behavior. Acta Biomater 2013;9:8037–8045.
5. Wang M. Developing bioactive composite materials for tissue replacement. Biomaterials 2003;24:2133–2151.
6. Ohtsuki C, Kamitakahara M, Miyazaki T. Bioactive ceramic-based materials with designed reactivity for bone tissue regeneration. J R Soc Interface 2009;6(Suppl 3):S349–360.
7. Tampieri A, D'Alessandro T, Sandri M, Sprio S, Landi E, Bertinetti L, Panseri S, Pepponi G, Goettlicher J, Banobre-Lopez M, Rivas J. Intrinsic magnetism and hyperthermia in bioactive Fe-doped hydroxyapatite. Acta Biomater 2012;8:843–851.
8. Vlad MD, Şindilar EV, Mariñoso ML, Poeată I, Torres R, López J, Baracoa M, Fernandez E. Osteogenic biphasic calcium sulphate dihydrate/iron-modified α-tricalcium phosphate bone cement for spinal applications: *In vivo* study. Acta Biomater 2010;6:607–616.
9. Kokubo T, Kim HM, Kawashita M. Novel bioactive materials with different mechanical properties. Biomaterials 2003;24:2161–2175.
10. Kokubo T, Kim HM, Kawashita M, Nakamura T. Bioactive metals: Preparation and properties. J Mater Sci-Mater Med 2004;15:99–107.
11. Ignatius AA, Augat P, Hollstein E, Schorlemmer S, Peraus M, Pokinskyj P, Claes L. Biocompatibility and functionality of the degradable polymer alkylene bis(dilactoyl)-methacrylate for screw augmentation *in vivo*. J Biomed Mater Res B 2005;75:128–136.
12. Sun L, Hu YY, Xiong Z, Wang WM, Pan Y. Repair of the radial defect of rabbit with polyester/tricalcium phosphate scaffolds prepared by rapid prototyping technology. Chin J Traumatol 2006;9:298–302.
13. Yu D, Li Q, Mu X, Chang T, Xiong Z. Bone regeneration of critical calvarial defect in goat model by PLGA/TCP/rhBMP-2 scaffolds prepared by low-temperature rapid-prototyping technology. Int J Oral Max Surg 2008;37:929–934.
14. Wen Z, Zhang L, Chen C, Liu Y, Wu C, Dai C. A construction of novel iron-foam-based calcium phosphate/ chitosan coating biodegradable scaffold material. Mater Sci Eng C Mater Biol Appl 2013;33:1022–1031.
15. Chen H, Zhang E, Yang K. Microstructure, corrosion properties and bio-compatibility of calcium zinc phosphate coating on pure iron for biomedical application. Mater Sci Eng C Mater Biol Appl 2014;34:201–206.
16. Witte F, Feyerabend F, Maier P, Fischer J, Störmer M, Blawert C, Dietzel W, Hort N. Biodegradable magnesium–hydroxyapatite metal matrix composites. Biomaterials 2007;28:2163–2174.
17. Yu K, Chen L, Zhao J, Li S, Dai Y, Huang Q, Yu Z. *In vitro* corrosion behavior and *in vivo* biodegradation of biomedical β-Ca3(PO4)2/Mg–Zn composites. Acta Biomater 2012;8:2845–2855.
18. Yu K, Chen L, Zhao J, Wang R, Dai Y, Huang Q. *In vivo* biocompatibility and biodegradation of a Mg-15%Ca3(PO4)2 composite as an implant material. Mater Lett 2013;98:22–25.
19. Cheng J, Huang T, Zheng YF. Microstructure, mechanical property, biodegradation behavior, and biocompatibility of biodegradable Fe–Fe2O3 composites. J Biomed Mater Res A 2013;102:2277–2287.
20. Ulum MF, Arafat A, Noviana D, Yusop AH, Nasution AK, Abdul Kadir MR, Hermawan H. *In vitro* and *in vivo* degradation evaluation of novel iron-bioceramic composites for bone implant applications. Mater Sci Eng C Mater Biol Appl 2014;36:336–344.
21. De Aza PN, Luklinska ZB, Santos C, Guitian F, De Aza S. Mechanism of bone-like formation on a bioactive implant *in vivo*. Biomaterials 2003;24:1437–1445.
22. Noviana D, Nasution AK, Ulum MF, Hermawan H. Degradation of Fe-bioceramic composites at two different implantation sites in sheep animal model observed by X-ray radiography. Eur Cells Mater 2013;26(Suppl 5):S56.
23. Gerald M, Denise S. A Practical Guide to Decontamination in Healthcare. New York: Wiley; 2012. pp 325.
24. Pearce AI, Richards RG, Milz S, Schneider E, Pearce SG. Animal models for implant biomaterial research in bone: A review. Eur Cells Mater 2007;13:1–10.
25. Kuzyk PR, Schemitsch EH. The basic science of peri-implant bone healing. Indian J Orthop 2011;45:108–115.
26. Ducheyne P, Qiu Q. Bioactive ceramics: The effect of surface reactivity on bone formation and bone cell function. Biomaterials 1999;20:2287–2303.
27. Macfarlane PS, Reid R, Callander R. Pathology Illustrated, 5th ed. Edinburgh: Churchill Livingstone; 2000.
28. Teefey SA, Middleton WD, Patel V, Hildebolt CF, Boyer MI. The accuracy of high-resolution ultrasound for evaluating focal lesions of the hand and wrist. J Hand Surg-Am 2004;29:393–399.
29. Tchelepi H, Ralls PW. Color comet-tail artifact: Clinical applications. Am J Roentgenol 2009;192:11–18.
30. Rojbani H, Nyan M, Ohya K, Kasugai S. Evaluation of the osteoconductivity of alpha-tricalcium phosphate, beta-tricalcium phosphate, and hydroxyapatite combined with or without simvastatin in rat calvarial defect. J Biomed Mater Res A 2011;98:488–498.
31. Wood RC, LeCluyse EL, Fix JA. Assessment of a model for measuring drug diffusion through implant-generated fibrous capsule membranes. Biomaterials 1995;16:957–959.
32. Erdmann N, Bondarenko A, Hewicker-Trautwein M, Angrisani N, Reifenrath J, Lucas A, Meyer-Lindenberg A. Evaluation of the soft tissue biocompatibility of MgCa0.8 and surgical steel 316L *in vivo*: A comparative study in rabbits. Biomed Eng Online 2010;9:63.
33. Lange T, Schilling AF, Peters F, Haag F, Morlock MM, Rueger JM, Amling M. Proinflammatory and osteoclastogenic effects of beta-tricalciumphosphate and hydroxyapatite particles on human mononuclear cells *in vitro*. Biomaterials 2009;30:5312–5318.
34. Puleo DA, Nanci A. Understanding and controlling the bone-implant interface. Biomaterials 1999;20:2311–2321.
35. Ulum MF, Paramitha D, Estuningsih S, Noviana D, Hermawan H. Metal ion level and polymorphonuclear leukocyte cells number as determination factors for early *in vivo* rejection of biodegradable metals. Eur Cells Mater 2013;26(Suppl 5):S59.
36. Al-Saffar N, Revell PA. Pathology of the bone-implant interfaces. J Long-Term Eff Med Impl 1999;9:319–347.
37. Kubies D, Himmlova L, Riedel T, Chanova E, Balik K, Douderova M, Bartova J, Pesakova V. The interaction of osteoblasts with bone-implant materials: 1. The effect of physicochemical surface properties of implant materials. Physiol Res 2011;60:95–111.
38. Ambore B, Ravikanth K, Maini S, Rekhe DS. Haematological profile and growth performance of goats under transportation stress. Vet World 2009;2:195–198.
39. Kannan G, Terrill TH, Kouakou B, Gazal OS, Gelaye S, Amoah EA, Samake S. Transportation of goats: Effects on physiological stress responses and live weight loss. J Anim Sci 2000;78:1450–1457.
40. Langton DJ, Sidaginamale RP, Joyce TJ, Natu S, Blain P, Jefferson RD, Rushton S, Nargol AV. The clinical implications of elevated blood metal ion concentrations in asymptomatic patients with MoM hip resurfacings: A cohort study. BMJ Open 2013;3:e001541.
41. Ramírez-Pérez AH, Buntinx SE, Rosiles R. Effect of breed and age on the voluntary intake and the micromineral status of non-pregnant sheep: II. Micromineral status. Small Ruminant Res 2000;37:231–242.
42. Walwadkar SD, Suryakar AN, Katkam RV, Kumbar KM, Ankush RD. Oxidative stress and calcium-phosphorus levels in Rheumatoid arthritis. Indian J Clin Biochem 2006;21:134–137.
43. Conz MB, Granjeiro JM, Soares Gde A. Hydroxyapatite crystallinity does not affect the repair of critical size bone defects. J Appl Oral Sci 2011;19:337–342.
44. Scholtysek C, Kronke G, Schett G. Inflammation-associated changes in bone homeostasis. Inflamm Allergy Drug Targets 2012;11:188–195.
45. Schmutz P, Quach-Vu N-C, Gerber I. Metallic medical implants: Electrochemical characterization of corrosion processes. Interface 2008;17:35–40.
46. Kannan MB, Raman RKS. *In vitro* degradation and mechanical integrity of calcium-containing magnesium alloys in modified-simulated body fluid. Biomaterials 2008;29:2306–2314.

47. Bengtsson Å, Shchukarev A, Persson P, Sjöberg S. A solubility and surface complexation study of a non-stoichiometric hydroxyapatite. Geochim Cosmochim Acta 2009;73:257–267.
48. Carrodeguas RG, De Aza S. α-Tricalcium phosphate: Synthesis, properties and biomedical applications. Acta Biomater 2011;7:3536–3546.
49. Watanabe T. Wettability of ceramic surfaces -A wide range control of surface wettability from super hydrophilicity to super hydrophobicity, from static wettability to dynamic wettability. J Ceram Soc Jpn 2009;117:1285–1292.
50. Pedersen A, Hermansson M. Inhibition of metal corrosion by bacteria. Biofouling 1991;3:1–11.
51. Martínez IM, Meseguer-Olmo L, Bernabeu-Esclapez A, Velásquez PA, De Aza PN. *In vitro* behavior of α-tricalcium phosphate doped with dicalcium silicate in the system Ca2SiO4–Ca3(PO4)2. Mater Charact 2012;63:47–55.
52. Shalabi MM, Wolke JG, Jansen JA. The effects of implant surface roughness and surgical technique on implant fixation in an *in vitro* model. Clin Oral Implan Res 2006;17:172–178.
53. Suzuki K, Aoki K, Ohya K. Effects of surface roughness of titanium implants on bone remodeling activity of femur in rabbits. Bone 1997;21:507–514.
54. Liu B, Lun DX. Current application of beta-tricalcium phosphate composites in orthopaedics. Orthop Surg 2012;4:139–144.
55. Zhou AJ, Peel SA, Clokie CM. An evaluation of hydroxyapatite and biphasic calcium phosphate in combination with pluronic F127 and BMP on bone repair. J Craniofac Surg 2007;18:1264–1275.
56. Hermawan H, Dubé D, Mantovani D. Degradable metallic biomaterials: Design and development of Fe–Mn alloys for stents. J Biomed Mater Res A 2010;93:1–11.
57. Waksman R, Pakala R, Baffour R, Seabron R, Hellinga D, Tio FO. Short-term effects of biocorrodible iron stents in porcine coronary arteries. J Interv Cardiol 2008;21:15–20.
58. Peuster M, Wohlsein P, Brugmann M, Ehlerding M, Seidler K, Fink C, Brauer H, Fischer A, Hausdorf G. A novel approach to temporary stenting: Degradable cardiovascular stents produced from corrodible metal-results 6–18 months after implantation into New Zealand white rabbits. Heart 2001;86:563–569.
59. Peuster M, Hesse C, Schloo T, Fink C, Beerbaum P, von Schnakenburg C. Long-term biocompatibility of a corrodible peripheral iron stent in the porcine descending aorta. Biomaterials 2006;27:4955–4962.
60. Ajeesh M, Francis BF, Annie J, Harikrishna Varma PR. Nano iron oxide-hydroxyapatite composite ceramics with enhanced radiopacity. J Mater Sci-Mater Med 2010;21:1427–1434.
61. Gross KA, Jackson R, Cashion JD, Rodriguez-Lorenzo LM. Iron substitute apatites: A resorbable biomaterial with potential magnetic properties. Eur Cells Mater 2002;3(Suppl 2):114–117.
62. Hou CH, Hou SM, Hsueh YS, Lin J, Wu HC, Lin FH. The *in vivo* performance of biomagnetic hydroxyapatite nanoparticles in cancer hyperthermia therapy. Biomaterials 2009;30:3956–3960.

Evidences of in vivo bioactivity of Fe-bioceramic composites

ORIGINALITY REPORT

5%	0%	5%	0%
SIMILARITY INDEX	INTERNET SOURCES	PUBLICATIONS	STUDENT PAPERS

MATCH ALL SOURCES (ONLY SELECTED SOURCE PRINTED)

6%

★ M.F. Ulum, A. Arafat, D. Noviana, A.H. Yusop, A.K. Nasution, M.R. Abdul Kadir, H. Hermawan. "In vitro and in vivo degradation evaluation of novel iron-bioceramic composites for bone implant applications", Materials Science and Engineering: C, 2014

Publication

Exclude quotes	On	Exclude matches	< 3%
Exclude bibliography	On		